Exploring five methods for estimating net community production on the Siberian continental shelf and slope of the Arctic Ocean

M. B. Alkire[1], I. Polyakov[2], and R. W. Macdonald[3]

[1*]School of Oceanography, University of Washington, Seattle, WA USA
[2]International Arctic Research Center, University of Alaska Fairbanks, Fairbanks, AK USA
[3]Department of Fisheries & Oceans, Institute of Ocean Sciences, Sidney, BC Canada

[*]Corresponding author e-mail: alkirem@uw.edu

Supporting Information

Text S1. Operation and calibration of the Satlantic Ultraviolet Nitrate Analyzer (SUNA)

The SUNA instrument measures the ultraviolet (217-240 nm) absorbance of seawater across the probe's 1 cm path length approximately once per second. After every 10 samples, the SUNA records a dark absorbance reading (shutter closed to light source) to track any drift in instrument background. The raw spectral readings were archived by the SUNA internal memory in separate data files for each station with timestamps from the instrument's internal clock. In addition to nitrate, other inorganic ions absorb ultraviolet light in the spectral range measured by the SUNA. Absorption due to bromide is the most significant of these ions in open ocean conditions, although nitrite and sulfide may also be important in regions of oxygen depletion. Unlike nitrate, absorption due to bromide is temperature-dependent; thus it is recommended that the raw spectra be corrected for temperature effects on the bromide absorption by incorporating *in-situ* temperature and salinity data to estimate and remove the bromide absorption spectra [*Sakamoto et al*., 2009]. Since the raw spectra were stored only on the SUNA internal memory, these data must be synchronized with the CTD data record during post-processing in order to correct for the bromide absorption.

The SUNA instrument was mounted such that the volume channel was oriented vertically, allowing for free flow of water through the "sample volume" as the carousel moved downward through the water column. Although the SUNA was not actively pumped, this orientation maximized free flow through the sample channel. Since the sample volume of the SUNA was not plumbed to the CTD, no advance of the data stream is necessary to align the absorption spectra with the associated CTD data. Instead, the synchronization of the two data records was assured by comparing the timestamps of the two instruments and the nitrate concentrations reported in both in the SUNA and CTD data files. Prior to the start of the cruise, the SUNA clock (GMT time) was synchronized to a handheld GPS unit. During the cruise, the SUNA clock was compared against the NMEA that was used to provide time (also in GMT), latitude, and longitude to the CTD deck unit. The SUNA and NMEA/CTD clocks agreed to within 3 seconds.

Once synchronization was completed, the CTD data was interpolated to match the sampling frequency (~0.9 Hz) of the SUNA. This resulted in a combined data file with approximately one-second resolution in time for each cast. These data files were then processed using a program (ISUSDataProcessor) developed by Ken Johnson (MBARI) that corrects the spectral data for temperature effects on the bromide absorption and applies a linear baseline correction to account for absorption by colored dissolved organic matter [*Sakamoto et al*., 2009]. A calibration file, after adaptation to be used with ISUSDataProcessor, was used for all post-processing of the data. The calibration was checked intermittently during the cruise using distilled water and was found to be relatively stable. Each nitrate concentration calculated by this program has an associated fit-error (RMS deviation of observed nitrate absorbance from modeled values). Any concentrations with fit-errors exceeding 0.002 were omitted from the final data files to accommodate known instrumental noise [Ken Johnson, personal communication]. Finally, all CTD and SUNA data were interpolated onto a regular grid with 2 m intervals.

SUNA-derived nitrate concentrations can be biased due to instrument drift, specifically the drift of the baseline/reference spectrum associated with zero nitrate concentration. Additional biases can be introduced due to a failure to clean instrument optics prior to each deployment, insufficient power delivered to the instrument by the battery pack, and problems during attempts to recalibrate the instrument (*e.g.*, bubbles in the path length).

To correct for these potential errors, the SUNA nitrate concentrations were compared with select nitrate concentrations measured from discrete seawater samples collected at various depths. Uncertainties associated with the matching of the SUNA and CTD data due to imperfect time synchronization, bin averaging of temperature and salinity data used in the bromide absorption correction, and interpolation may also introduce errors into any applied correction. In attempt to mitigate such mismatches, comparisons were restricted to depths $\leq$ 20 m and $\geq$ 300 m, where the change in nitrate concentration with depth was minimal. An additional filter was applied to data used in the calibration, such that differences between SUNA- and bottle-derived nitrate concentrations > 2 mmol m^{-3} were excluded from the analysis.

Simple, linear regressions were computed between the SUNA-derived and sampled-derived nitrate concentrations and the resulting regressions coefficients used to correct the SUNA-derived nitrate concentrations accordingly.

Estimates uncertainties of SUNA-derived nitrate concentrations after these corrections were estimated to be < 1 mmol m^{-3}.

Table S1. Mean estimates of net community production from the five different methods (A, B, D, E, and G), averaged along the transects (Severnaya Zemlya, Laptev Sea, Lomonosov Ridge, and East Siberian Sea) shown in Fig. 1. Note that these estimates were not adjusted for the influence of meteoric water and sea ice melt.

Severnaya Zemlya Transect																
	2013	2013	2013	2013	2015	2015	2015	2015					ALL YRS			
	Low CI	Mean	Stdev	*High CI*	*Low CI*	Mean	Stdev	*High CI*					*Low CI*	Mean	Stdev	*High CI*
A	12.1	15.9	5.0	19.7	6.8	12.7	7.1	18.6					11.3	14.4	6.1	17.5
B	7.0	13.8	8.9	20.7	9.7	15.5	7.0	21.4					10.8	14.7	7.7	18.7
D	9.1	12.5	4.4	15.8	4.9	9.7	5.8	14.6					8.5	11.2	5.1	13.8
E	9.1	12.5	4.4	15.9	4.9	9.8	5.8	14.7					8.6	11.2	5.2	13.9
G	18.7	20.8	2.8	22.9	14.6	17.7	3.7	20.8					17.5	19.3	3.5	21.2
ALL METHODS	**13.4**	**15.2**	**5.9**	**16.9**	**11.0**	**13.1**	**6.5**	**15.2**					**12.8**	**14.2**	**6.3**	**15.5**
Eurasian Basin (Codispoti et al., 2013)	5-25															
Nansen Basin (Uflsbo et al., 2014)	5-25															
Laptev Transect																
	2013	2013	2013	2013	2015	2015	2015	2015	2018	2018	2018	2018	ALL YRS			
	Low CI	Mean	Stdev	*High CI*	*Low CI*	Mean	Stdev	*High CI*	*Low CI*	Mean	Stdev	*High CI*	*Low CI*	Mean	Stdev	*High CI*
A	*16.7*	19.1	4.2	*21.5*	*9.1*	11.1	3.9	*13.2*	*12.8*	14.6	3.3	*16.3*	13.3	14.8	4.9	16.2
B	*10.3*	13.5	5.6	*16.8*	*11.5*	12.4	1.7	*13.3*	*10.1*	11.3	2.1	*12.4*	11.3	12.4	3.7	13.5
D	*12.5*	14.0	2.5	*15.4*	*6.4*	8.0	3.0	*9.6*	*9.1*	10.3	2.3	*11.6*	9.6	10.6	3.5	11.7
E	*12.4*	14.5	3.6	*16.6*	*6.4*	8.0	3.0	*9.6*	*9.1*	10.3	2.3	*11.6*	9.6	10.8	4.0	12.0
G	*12.0*	13.6	2.8	*15.2*	*11.8*	12.8	1.8	*13.7*	*9.6*	10.5	1.7	*11.4*	11.5	12.2	2.5	13.0
ALL METHODS	**13.9**	**14.9**	**4.3**	**16.0**	**9.6**	**10.4**	**3.5**	**11.1**	**10.8**	**11.4**	**2.9**	**12.0**	**11.6**	**12.2**	**4.1**	**12.7**
ESS + Laptev Northern (Codispoti et al., 2013)	3-15															
Mendeleev Ridge (Uflsbo et al., 2014)	10-30															
Lomonosov Ridge Transect																
	2013	2013	2013	2013	2015	2015	2015	2015	2018	2018	2018	2018	ALL YRS			
	Low CI	Mean	Stdev	*High CI*	*Low CI*	Mean	Stdev	*High CI*	*Low CI*	Mean	Stdev	*High CI*	*Low CI*	Mean	Stdev	*High CI*
A	13.7	15.3	1.9	16.9	11.8	13.2	1.8	14.6	13.7	15.5	2.4	17.2	13.8	14.7	2.2	15.5
B	9.2	13.1	4.6	17.0	12.4	14.5	2.8	16.6	10.6	12.5	2.7	14.5	11.9	13.3	3.5	14.6
D	9.8	10.8	1.2	11.8	8.9	10.0	1.5	11.2	9.5	10.7	1.7	12.0	9.9	10.5	1.5	11.1
E	9.8	10.9	1.2	11.9	8.9	10.0	1.5	11.2	9.5	10.8	1.8	12.0	9.9	10.5	1.5	11.2
G	8.6	9.3	0.8	10.0	10.8	12.1	1.7	13.4	9.1	10.0	1.2	10.8	9.8	10.5	1.7	11.2
ALL METHODS	**10.9**	**11.9**	**3.1**	**12.9**	**11.1**	**11.8**	**2.4**	**12.5**	**11.1**	**11.9**	**2.8**	**12.7**	**11.4**	**11.8**	**2.8**	**12.3**
Makarov Basin (Uflsbo et al., 2014)	0-20															
East Siberian Sea Transect																
					2015	2015	2015	2015	2018	2018	2018	2018	ALL YRS			
					Low CI	Mean	Stdev	*High CI*	*Low CI*	Mean	Stdev	*High CI*	*Low CI*	Mean	Stdev	*High CI*
A					19.5	20.4	1.5	21.3	20.5	23.4	4.1	26.3	20.3	21.7	3.2	23.1
B					-	-	-	-	7.2	12.6	7.5	18.0	9.3	12.6	7.5	15.9
D					15.8	16.5	1.2	17.2	16.2	17.6	2.0	19.1	16.3	17.0	1.7	17.7
E					15.8	16.6	1.2	17.3	16.6	18.7	3.0	20.9	16.5	17.5	2.4	18.6
G					14.2	21.0	11.3	27.8	5.9	9.7	5.4	13.5	11.3	15.9	10.6	20.5
ALL METHODS					**17.1**	**18.6**	**5.8**	**20.0**	**14.5**	**16.4**	**6.7**	**18.3**	**16.3**	**17.5**	**6.3**	**18.7**
ESS + Laptev Southern (Codispoti et al., 2013)	5-30															
Amundsen/Nansen Eastern (Uflsbo et al., 2014)	0-15															

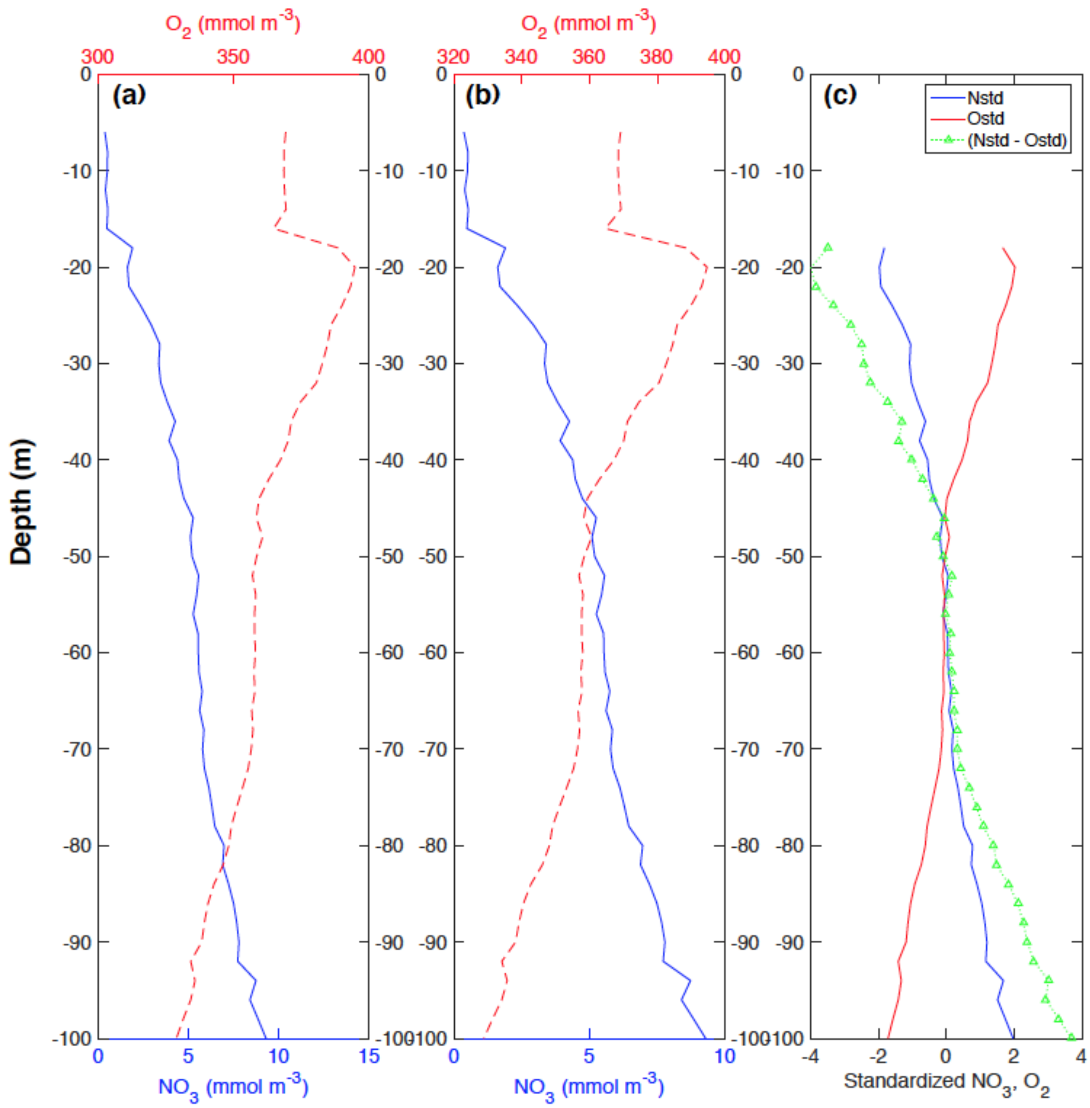

Figure S1. Vertical profiles of nitrate (NO_3) and dissolved oxygen (O_2) at station 15, occupied along the Laptev Sea section (~126ºE) during the 2015 NABOS cruise. Only the top 100 m of the profiles are shown. In the left panel, NO_3 (blue, solid line) and O_2 (red, dashed line) are plotted with the axes ranges set to between 0 and 15 mmol m^{-3} for NO_3 and 300 and 400 mmol m^{-3} for O_2. The apparent intersection depth is ~80 m. In the middle panel, the axes ranges are set to 0 and 10 mmol m^{-3} for NO_3 and 320 and 400 mmol m^{-3} for O_2; the apparent intersection depth is ~45 m. These two examples show how the apparent intersection depth can vary depending on the set axes limits. To remove this uncertainty, the NO_3 and O_2 profiles were put on the same axes using standardization (right panel). The point of intersection was determined by calculating the minimum absolute value of the difference between the standardized NO_3 (Nstd, blue line) and O_2 (Ostd, red line) profiles.

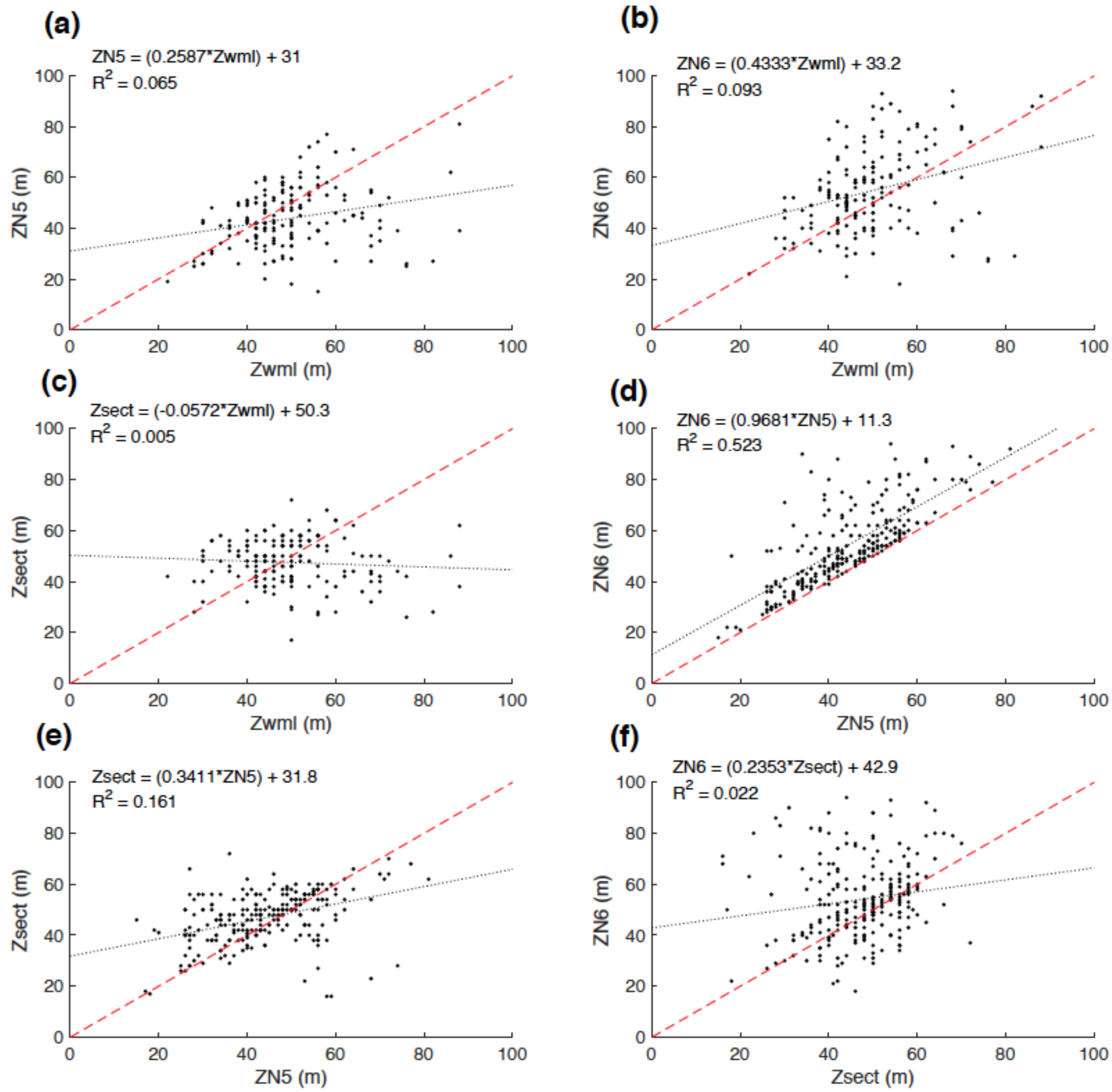

Figure S2. Linear regressions of integration depths comparing: (a) Zwml and ZN5; (b) Zwml and ZN6; (c) Zwml and Zsect; (d) ZN5 and ZN6; (e) ZN5 and Zsect; and (f) Zsect and ZN6. The equation and associated correlation coefficient are given for each regression in the top left of each panel. The lines corresponding to each regression are drawn as black, solid lines in each panel. For comparison, a 1:1 line is also plotted as a red, dashed line.

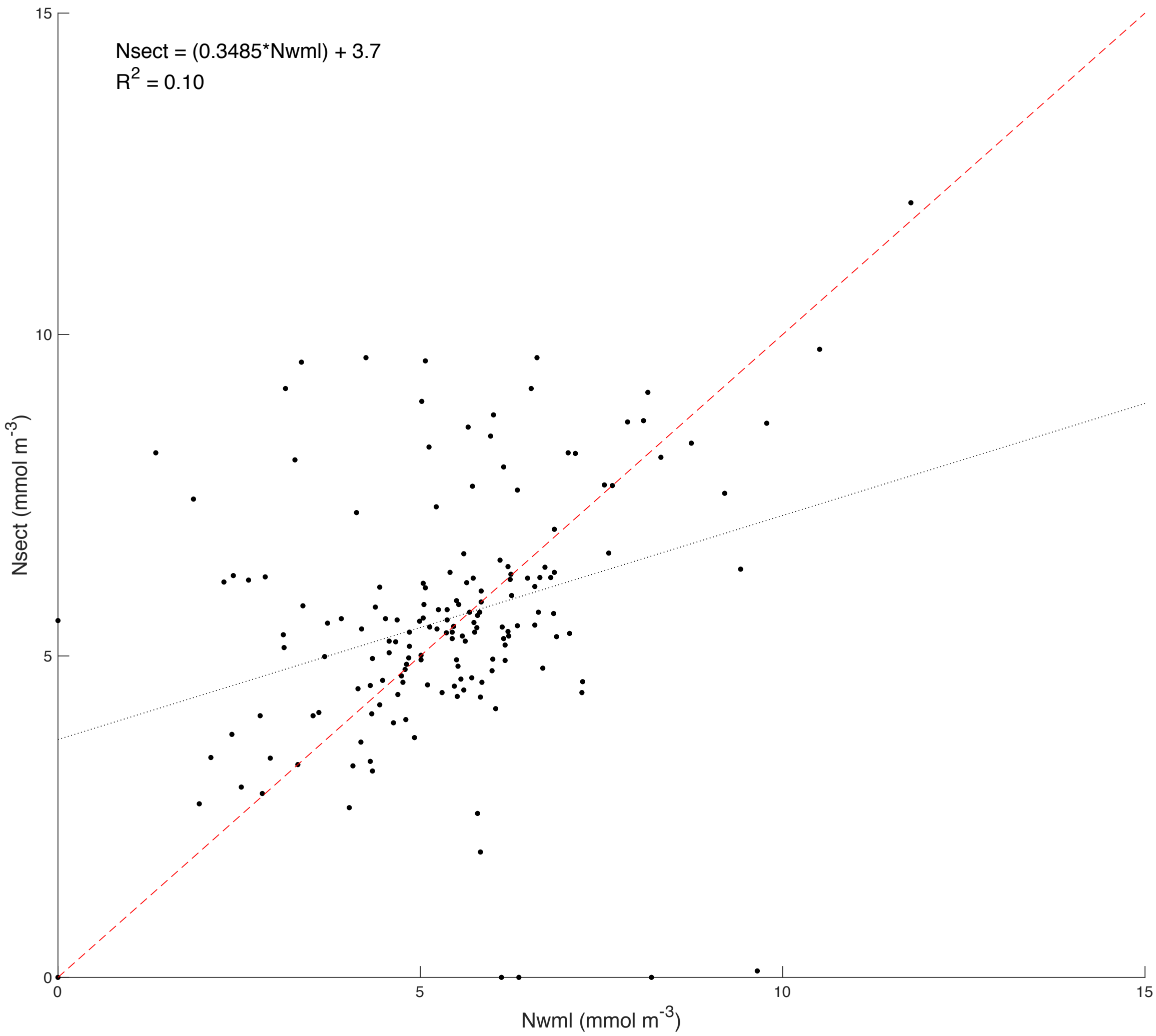

Figure S3. Linear regression of Nwml vs. Nsect. The equation and correlation coefficient of the regression are given in the upper left-hand corner of the plot. The solid black line shows the regression whereas the red, dashed line indicates a 1:1 relationship.

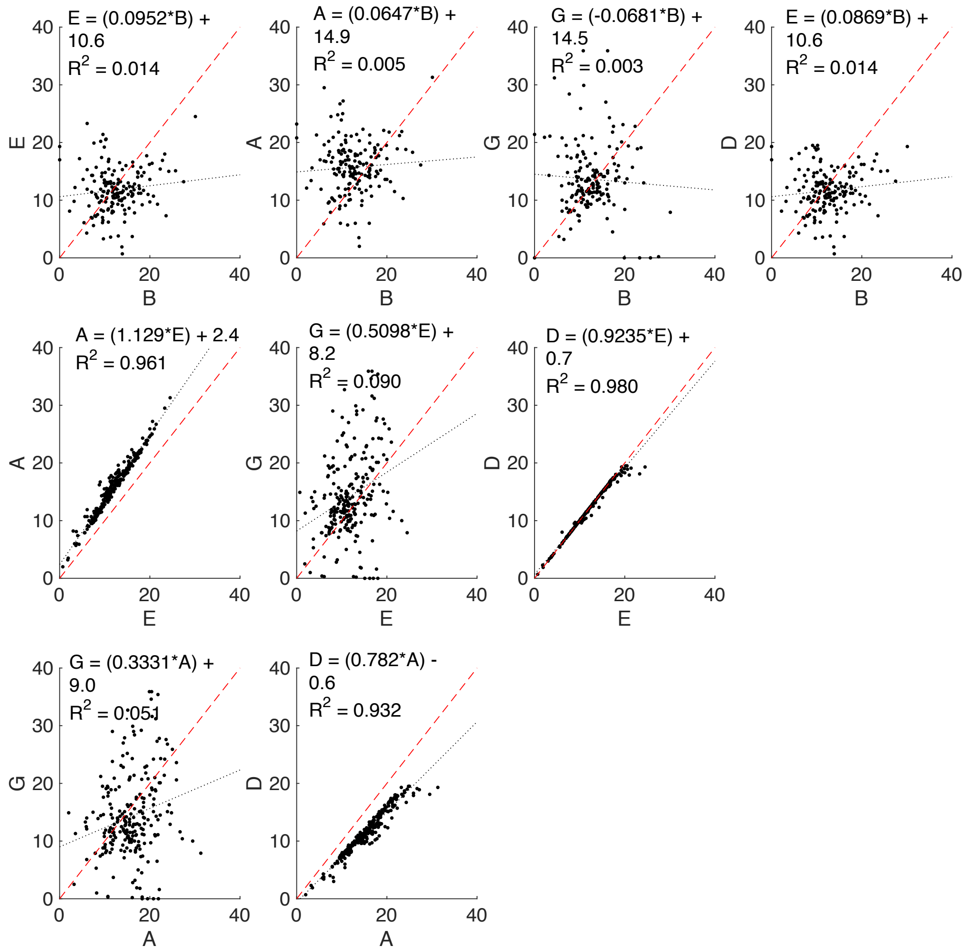

Figure S4. Linear regressions comparing the five different methods of calculating net community production. The top row compares the B method (x-axis) against the E, A, G, and D methods (left to right). The middle row shows regressions of the E method (x-axis) against methods A, G, and D. The bottom row shows regressions of the A method (x-axis) against those of G and D. The regression equations and associated correlation coefficients are provided in the top left of each panel. Also plotted in each panel are the regression lines (black, dotted line) and the 1:1 line (red, dashed line).

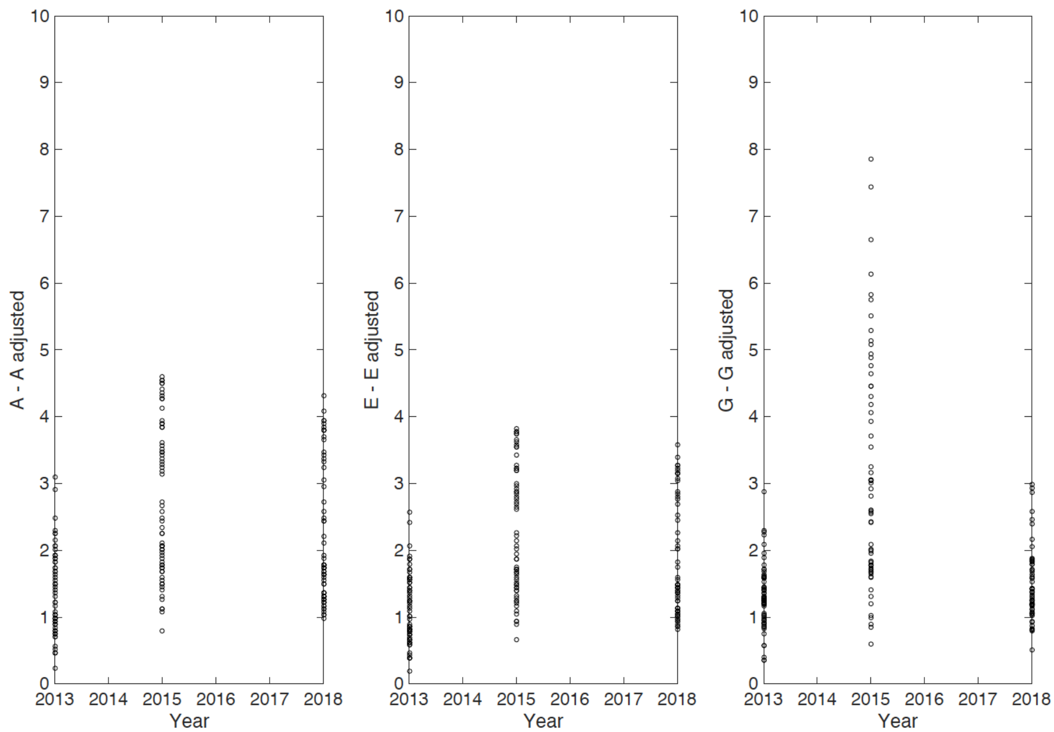

Figure S5. Differences in NCP estimates A (left panel), E (middle panel), and G (right panel) before and after adjustment for the impact of meteoric water and sea ice meltwater on nitrate inventories; plotted against cruise year.

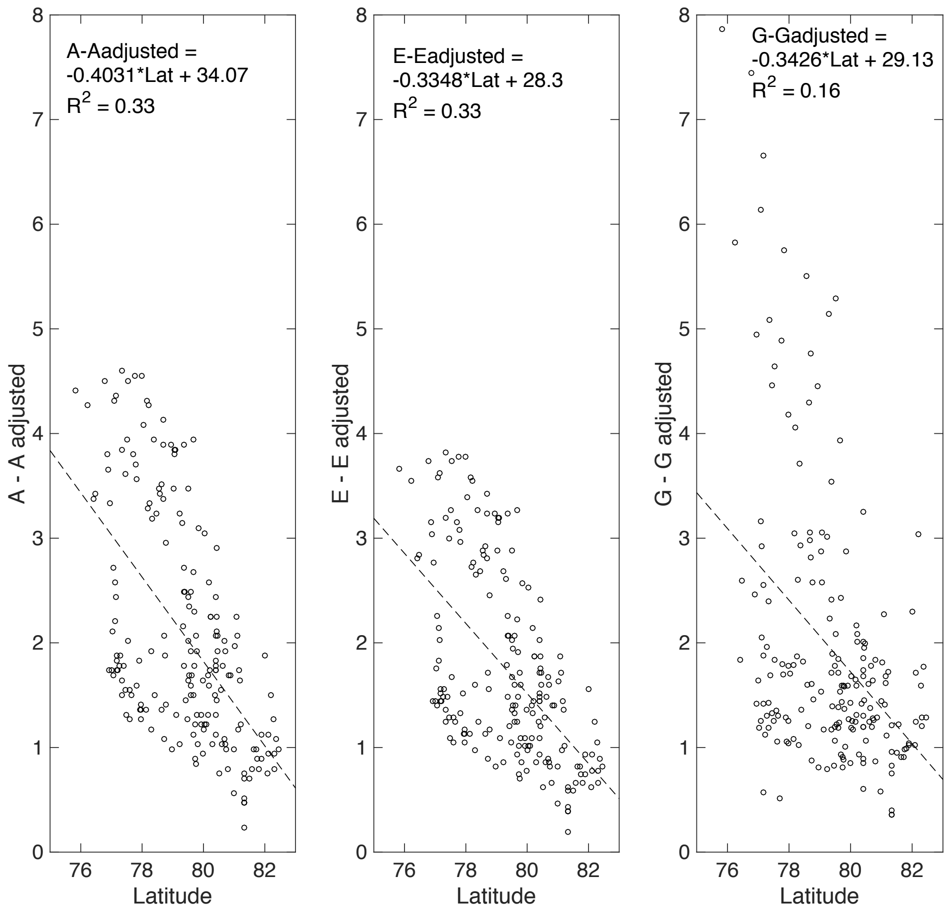

Figure S6. Regressions of latitude against the differences in NCP estimates A (left panel), E (middle panel), and G (right panel) before and after adjustment for the impact of meteoric water and sea ice meltwater on nitrate inventories. The regression equations and associated correlation coefficients are given at the top of each panel.

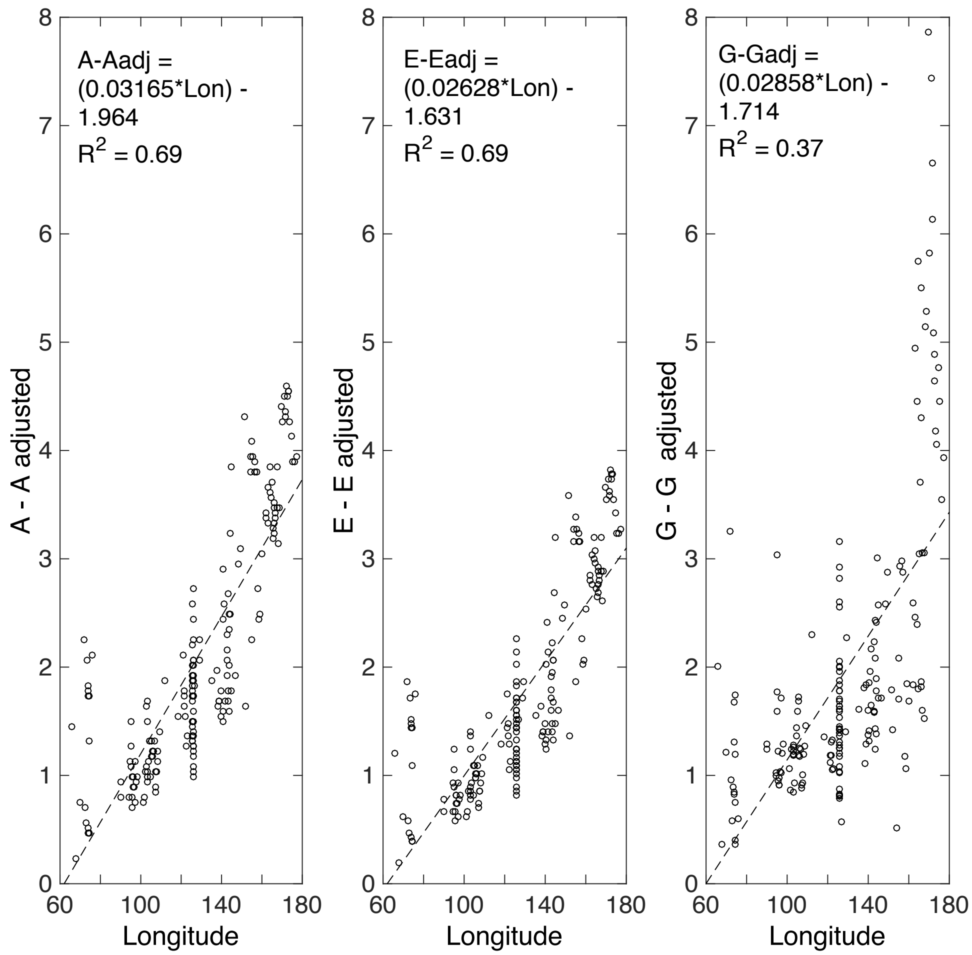

Figure S7. Regressions of longitude against the differences in NCP estimates A (left panel), E (middle panel), and G (right panel) before and after adjustment for the impact of meteoric water and sea ice meltwater on nitrate inventories. The regression equations and associated correlation coefficients are given at the top of each panel.

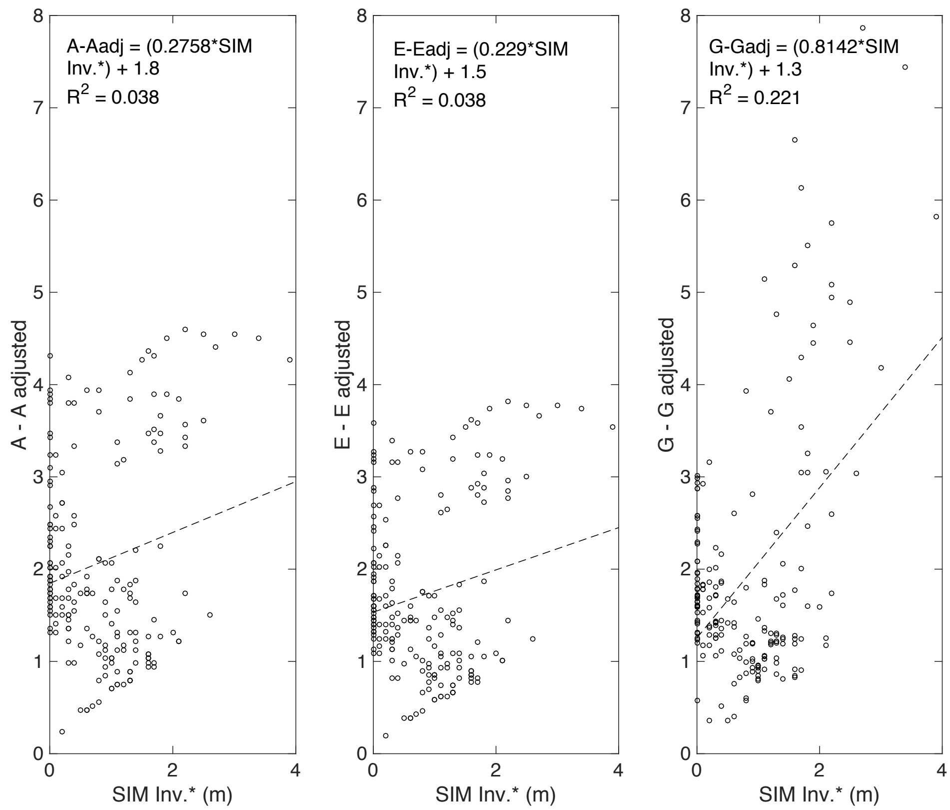

Figure S8. Regressions of positive sea ice meltwater inventories over the top 0-50 m (negative fractions were set to zero) against the differences in NCP estimates A (left panel), E (middle panel), and G (right panel) before and after adjustment for the impact of meteoric water and sea ice meltwater on nitrate inventories. The regression equations and associated correlation coefficients are given at the top of each panel.

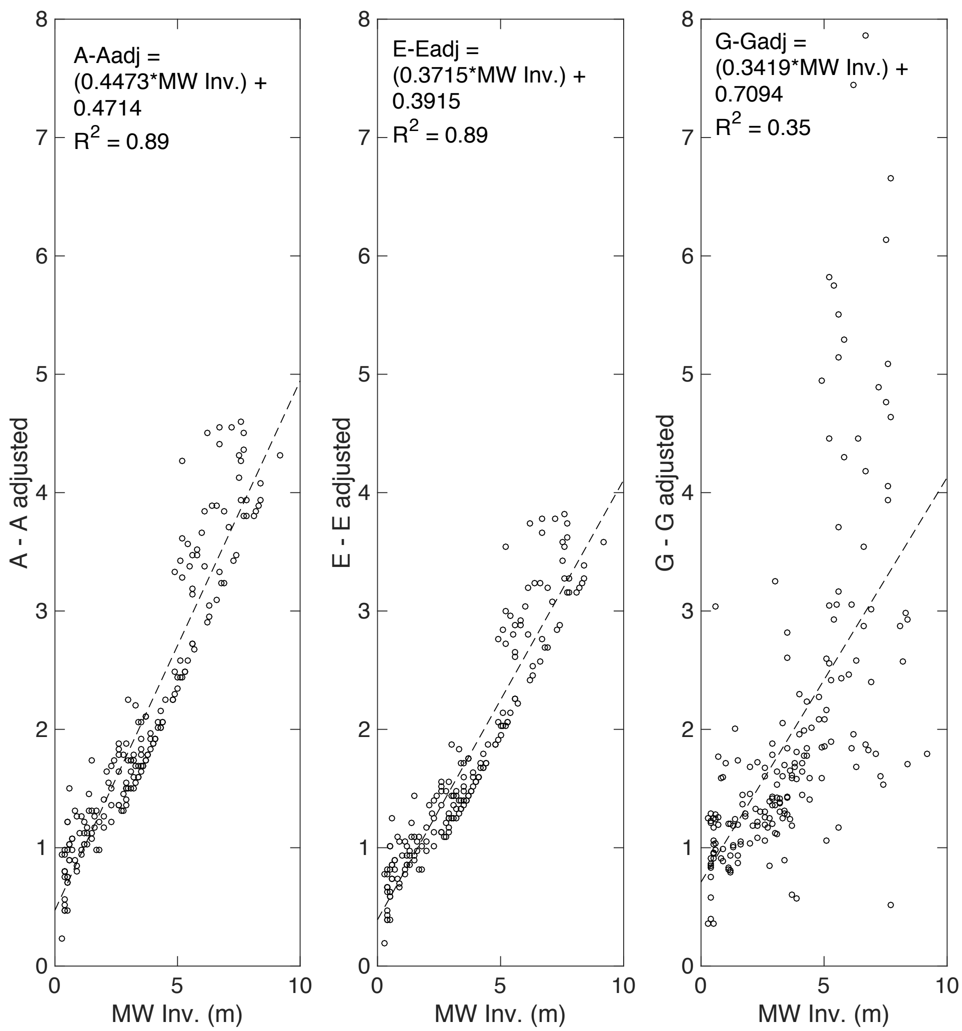

Figure S9. Regressions of positive meteoric water inventories over the top 0-50 m (negative fractions were set to zero) against the differences in NCP estimates A (left panel), E (middle panel), and G (right panel) before and after adjustment for the impact of meteoric water and sea ice meltwater on nitrate inventories. The regression equations and associated correlation coefficients are given at the top of each panel.

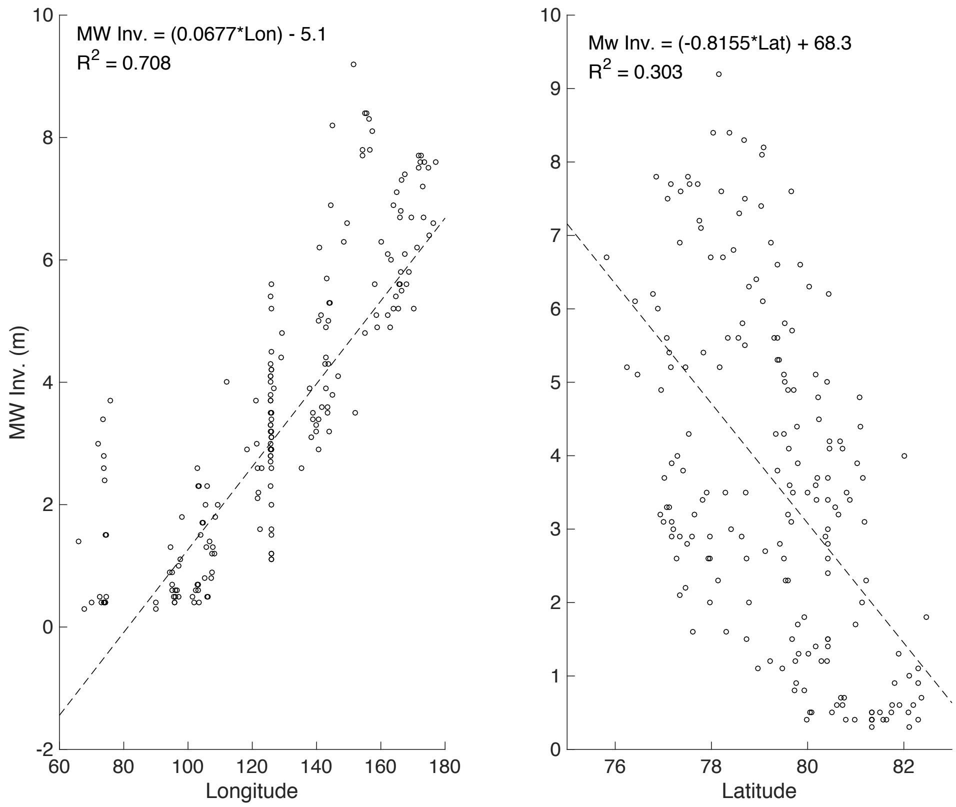

Figure S10. Regressions of positive meteoric water inventories over the top 0-50 m (negative fractions were set to zero) against longitude (left panel) and latitude (right panel). The regression equations and associated correlation coefficients are given at the top of each panel.

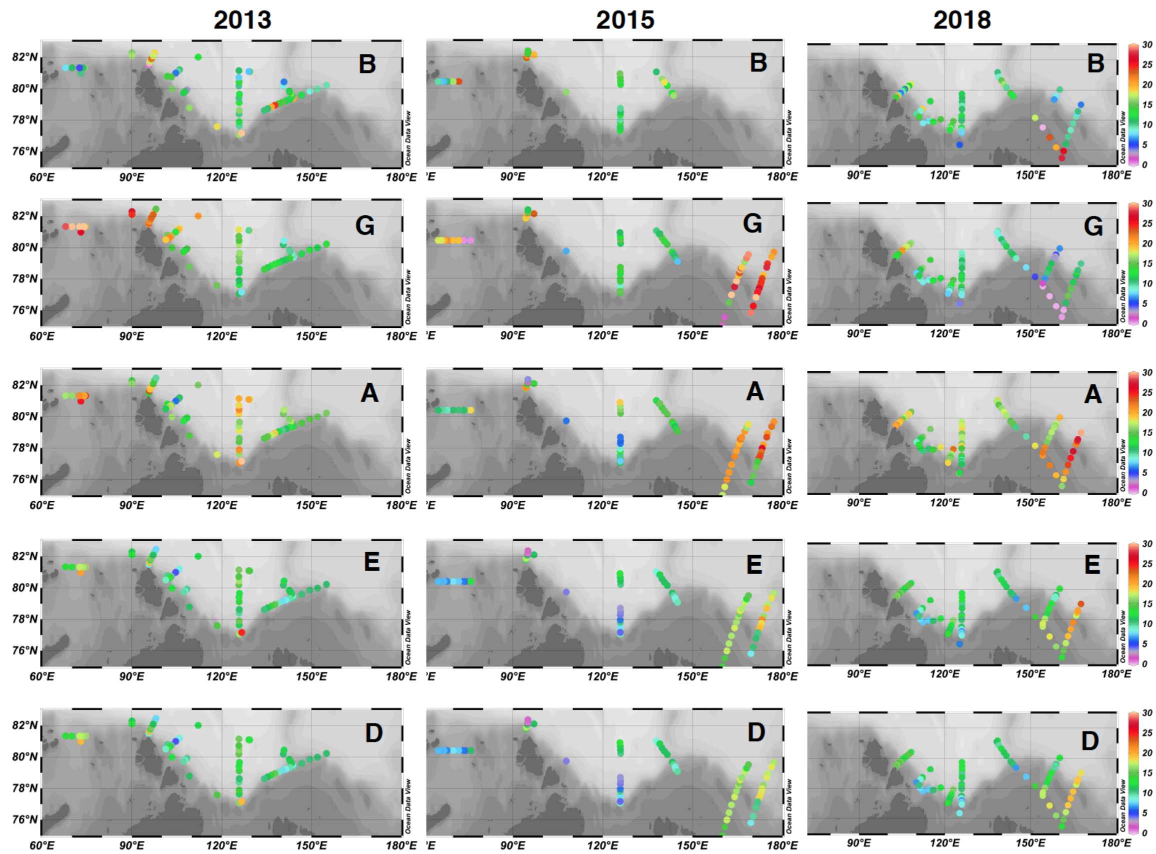

Figure S11. Maps of net community production estimates using the five different methods (B, top row; G, second row; A, third row; E, fourth row; and D, bottom row) for each cruise year: 2013 (left panels), 2015 (middle panels), and 2018 (right panels). Colorbars are equivalent among all panels, with ranges set between 0 (cooler colors) and 30 (warmer colors) g C m^{-2}. Note that these estimates were calculated without an adjustment for the impact of meteoric water and sea ice melt.

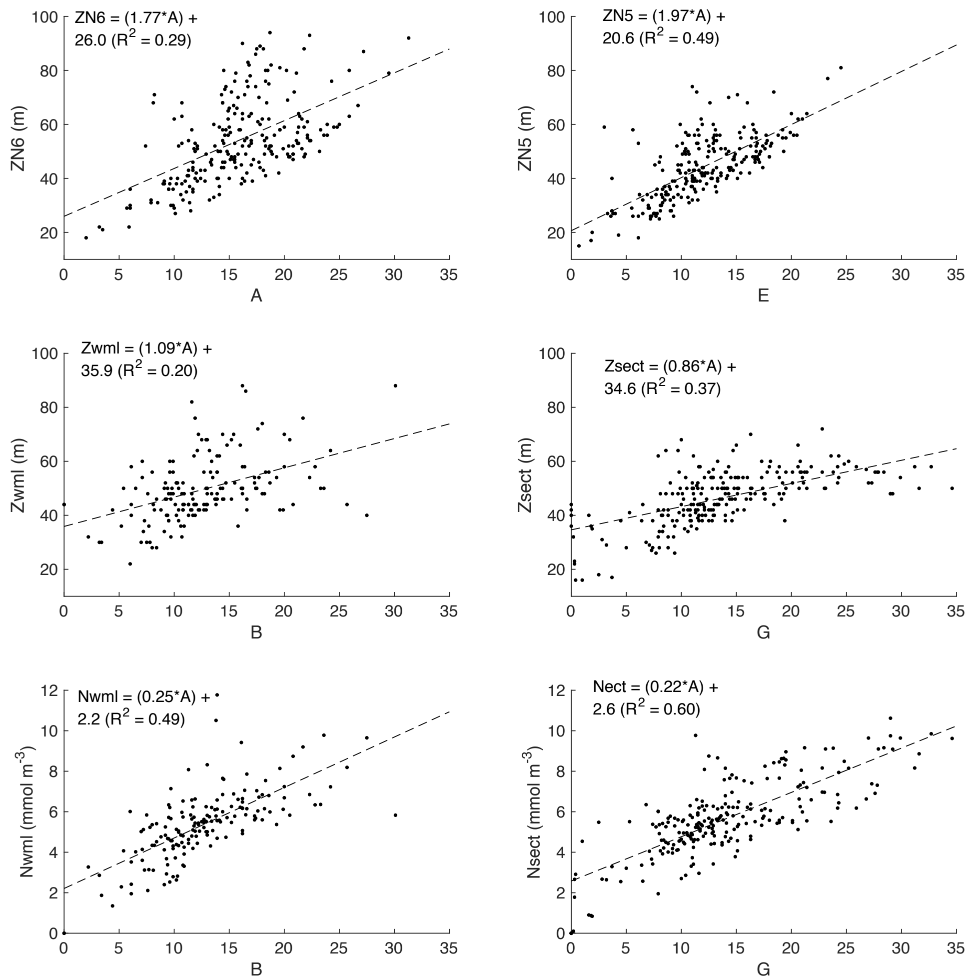

Figure S12. Linear regressions of net community production estimates (A, B, E, and G) against associated integration depths (ZN6, Zwml, ZN5, and Zsect) as well as pre-bloom nitrate concentrations (Zwml and Zsect). Equations for the corresponding regressions are given in each panel. No regressions were completed for estimate D because both the integration depth and pre-bloom nitrate concentration were assigned constant values.

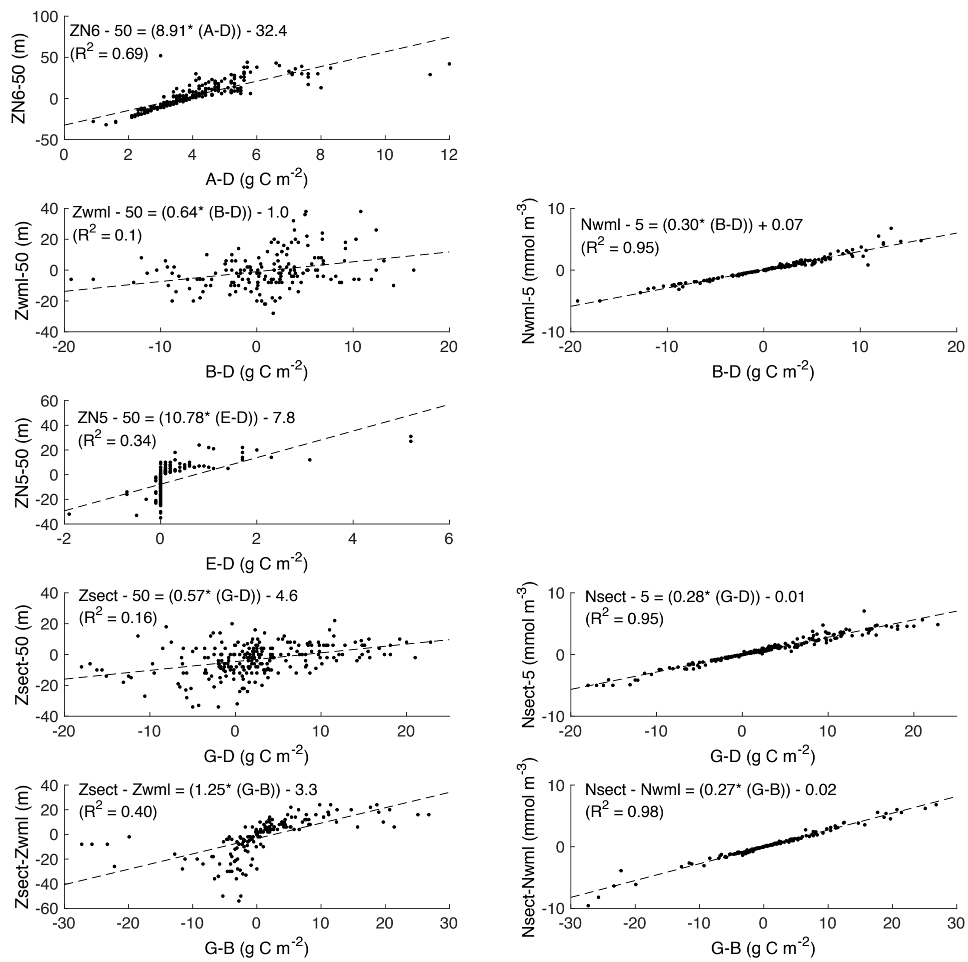

Figure S13. Regressions comparing the differences between net community production estimates against corresponding differences in the integration depth (left panels) and pre-bloom nitrate concentration (right panels). The D method was used as the main reference against which the other methods were compared. Recall that the integration depth (50 m) and pre-bloom nitrate concentration (5 mmol m^{-3}) were pre-assigned constant values for the D method. Methods B and G are also compared in the bottom panels. Equations for the linear regressions are given in each panel. Note the axes in each panel have different scales.